NASA/TM—2004-213085

Characterization of an Ultra-High Temperature Ceramic Composite

Stanley R. Levine and Elizabeth J. Opila
Glenn Research Center, Cleveland, Ohio

Raymond C. Robinson
QSS Group, Inc., Cleveland, Ohio

Jonathan A. Lorincz
Ohio University, Athens, Ohio

May 2004

The NASA STI Program Office . . . in Profile

Since its founding, NASA has been dedicated to the advancement of aeronautics and space science. The NASA Scientific and Technical Information (STI) Program Office plays a key part in helping NASA maintain this important role.

The NASA STI Program Office is operated by Langley Research Center, the Lead Center for NASA's scientific and technical information. The NASA STI Program Office provides access to the NASA STI Database, the largest collection of aeronautical and space science STI in the world. The Program Office is also NASA's institutional mechanism for disseminating the results of its research and development activities. These results are published by NASA in the NASA STI Report Series, which includes the following report types:

- TECHNICAL PUBLICATION. Reports of completed research or a major significant phase of research that present the results of NASA programs and include extensive data or theoretical analysis. Includes compilations of significant scientific and technical data and information deemed to be of continuing reference value. NASA's counterpart of peer-reviewed formal professional papers but has less stringent limitations on manuscript length and extent of graphic presentations.

- TECHNICAL MEMORANDUM. Scientific and technical findings that are preliminary or of specialized interest, e.g., quick release reports, working papers, and bibliographies that contain minimal annotation. Does not contain extensive analysis.

- CONTRACTOR REPORT. Scientific and technical findings by NASA-sponsored contractors and grantees.

- CONFERENCE PUBLICATION. Collected papers from scientific and technical conferences, symposia, seminars, or other meetings sponsored or cosponsored by NASA.

- SPECIAL PUBLICATION. Scientific, technical, or historical information from NASA programs, projects, and missions, often concerned with subjects having substantial public interest.

- TECHNICAL TRANSLATION. English-language translations of foreign scientific and technical material pertinent to NASA's mission.

Specialized services that complement the STI Program Office's diverse offerings include creating custom thesauri, building customized databases, organizing and publishing research results . . . even providing videos.

For more information about the NASA STI Program Office, see the following:

- Access the NASA STI Program Home Page at ***http://www.sti.nasa.gov***

- E-mail your question via the Internet to help@sti.nasa.gov

- Fax your question to the NASA Access Help Desk at 301–621–0134

- Telephone the NASA Access Help Desk at 301–621–0390

- Write to:
  NASA Access Help Desk
  NASA Center for AeroSpace Information
  7121 Standard Drive
  Hanover, MD 21076

NASA/TM—2004-213085

Characterization of an Ultra-High Temperature Ceramic Composite

Stanley R. Levine and Elizabeth J. Opila
Glenn Research Center, Cleveland, Ohio

Raymond C. Robinson
QSS Group, Inc., Cleveland, Ohio

Jonathan A. Lorincz
Ohio University, Athens, Ohio

National Aeronautics and
Space Administration

Glenn Research Center

May 2004

Acknowledgments

Thanks to Terry R. McCue for scanning electron microscopy support and Ronald E. Phillips for assistance with testing. Also, thanks to Dr. David Glass, NASA Langley Research Center, for providing the Starfire UHTCC plate and to Dr. Walter Sherwood, Starfire Systems, Inc., for providing processing details and for permission to present this study.

Available from

NASA Center for Aerospace Information
7121 Standard Drive
Hanover, MD 21076

National Technical Information Service
5285 Port Royal Road
Springfield, VA 22100

Available electronically at http://gltrs.grc.nasa.gov

Characterization of an Ultra-High Temperature Ceramic Composite

Stanley R. Levine and Elizabeth J. Opila
National Aeronautics and Space Administration
Glenn Research Center
Cleveland, Ohio 44135

Raymond C. Robinson
QSS Group, Inc.
Cleveland, Ohio 44135

Jonathan A. Lorincz
Ohio University
Athens, Ohio 45701

Summary

Ultra-high temperature ceramics (UHTC) are of interest for hypersonic vehicle leading edge applications. Monolithic UHTCs are of concern because of their low fracture toughness and brittle behavior. UHTC composites (UHTCC) are being investigated as a possible approach to overcome these deficiencies. In this study a small sample of a UHTCC was evaluated by limited mechanical property tests, furnace oxidation exposures, and oxidation exposures in a flowing environment generated by an oxy-acetylene torch. The composite was prepared from a carbon fiber preform using ceramic particulates and a preceramic polymer. Test results raised concerns about microcracking due to thermal expansion mismatch between the matrix and the carbon fiber reinforcements, and about the oxidation resistance of the HfB_2-SiC coating layer and the composite constituents. However, positive performance in the torch test warrants further study of this concept.

Introduction

The high melting points of refractory metal diborides coupled with their ability to form refractory oxide scales give these materials the capability to withstand temperatures in the 1900 to 2500 °C range.[1] These ultra-high temperature ceramics (UHTC) were developed in the 1960's.[2] Fenter[3] provides a comprehensive review of the work accomplished in the 1960's and early 1970's. Additions of silicon carbide are used to enhance oxidation resistance and limit diboride grain growth. Carbon is also sometimes used as an additive to enhance thermal stress resistance. These materials offer a good combination of properties that make them candidates for airframe leading edges on sharp-bodied reentry vehicles.[1] UHTC have some potential to perform well in the environment for such applications, i.e. air at low pressure. However, for hypersonic flight in the upper atmosphere one must recognize that stagnation pressures can be greater than one atmosphere. Thus their poor oxidation resistance can be an issue.[4] Unreliable behavior that results from low fracture toughness and large scatter in material properties is also an issue that can arise under severe thermal shock and gradient loads, or at attachments.[4]

At very high temperatures in a flowing environment most of the B_2O_3[5] and SiO_2[6] formed by oxidation will be lost by evaporation or active oxidation. Thus, the primary protective oxidation barrier for the refractory metal borides is the refractory metal oxide scale plus residual B_2O_3 and SiO_2 found in the interior of the oxide scale. In the case of ZrB_2 or HfB_2 we are dependent on ZrO_2 or HfO_2, respectively. Background information on these oxides can be found in the compilation edited by Alper.[7] These oxides, if perfect, would be good oxygen barriers. However, ZrO_2 and HfO_2 become nonstoichiometric by

forming oxygen lattice vacancies under low oxygen partial pressure conditions. They are also readily modified by aliovalent cations of lower valence to form oxygen lattice vacancies that allow rapid oxygen ion transport through the scale. So, from a chemistry perspective, ZrO_2 and HfO_2 are not good choices for a protective oxide scale. In addition, the volatile oxidation products cause the formation of a porous, permeable oxide scale. Another issue with ZrO_2 and HfO_2 scales is their phase instability. At high temperatures, ZrO_2 and HfO_2 are tetragonal. Upon cooling to room temperature they transform to the monoclinic structure with an attendant volume expansion. This phase transformation, coupled with their high thermal expansion coefficient and low thermal conductivity,[8] can easily lead to cracking and spalling under thermal transient conditions.

One means of possibly overcoming the reliability issue is to introduce fibers as a toughening and strengthening phase, and as a pathway to architectural tailoring of properties such as thermal conductivity, stiffness, strength, etc. Fiber choices at this time are limited to carbon. This introduces new problems such as the need for new processing approaches, oxidation of the reinforcing phase, and thermal expansion mismatch between the carbon fibers and the UHTC matrix to name just a few.

The purpose of this study was to examine UHTC composites (UHTCC) as an approach to resolving the reliability issue. Fiber reinforcement and functional grading are being examined to increase toughness and improve reliability. These approaches are being integrated with alloying approaches to improve oxidation resistance to develop UHTC materials with improved robustness for leading edge applications. The characterization and performance of one composite material approach for improving UHTC robustness is reported in this paper. A composite plate produced by Starfire Systems, Inc., Watervliet, New York, was examined in detail in the as-produced condition and after mechanical and oxidation tests. A caveat to keep in mind is that very little development effort went into this approach. A second objective of this study was to reveal some of the issues associated with the UHTCC concept.

Experimental Procedures

Materials

An ultra-high temperature ceramic composite plate (part number 000928–6–64) was produced by Starfire Systems, Inc. The constituents were Zoltek Panex® 30 carbon fabric PW06, Starfire Systems' SP-matrix polymer (allylhydridopolycarbosilane (AHPCS)), HfB_2 powder, and SiC powder. For the initial processing cycle the Zoltek cloth was cut into ~15 by ~15 cm (6 by 6 in.) pieces. Eleven plies were used; the bottom 6 layers of cloth were coated with SiC/AHPCS slurry and the top 5 layers were coated with HfB_2/AHPCS slurry. The coated cloth was put into an aluminum mold and pressed to ~12 MPa. The mold was clamped and cured under inert gas to 400 °C. The plate was removed from the mold and clamped between graphite plates and fired to 850 °C under inert gas to pyrolyze the AHPCS. Processing to 850 °C results in volatilization of about 95 percent of the potential pyrolysis products.[9]

Cycles 2 and 3 consisted of coating application of HfB_2/AHPCS slurry to the HfB_2 side of the plate. After each cycle the composite was clamped between graphite plates and fired to 850 °C under inert gas.

Cycles 4 through 10 consisted of vacuum infiltration with AHPCS only and pyrolysis to 850 °C under inert gas without clamping in a mold. The processed plate, shown in figure 1 had dimensions of 150 by 150 by 6 mm. The plate was trimmed and cut into flexure test specimens, oxidation coupons, and torch test coupons as shown in figure 2. As a result, specimen edges were not protected by matrix material.

One piece of scrap material was characterized in the as-produced condition using X-ray diffraction (XRD), optical microscopy of a polished cross-section, and scanning electron microscopy (SEM) of the as-produced surfaces and of the polished cross-section.

Flexural Tests

Five four point flexural tests were carried out at span to depth ratios of ~14 and ~16. Some tests were run with the HfB_2 side in tension and some tests were run with the C/SiC side in tension. A span to depth ratio of ~14 was initially achieved using a 40 mm inner span and an 80 mm outer span (the largest fixture available at the time). A span to depth ratio of ~16 was achieved using a 48 mm inner span and a 96 mm outer span fixture that was fabricated later. A span to depth of 16 is the minimum required by ASTM Standard C1341 for a proper composite flexural test.[10] Lower ratios drive the failure mode toward shear failures.

Furnace Oxidation

Oxidation coupons were 2.54 by 1.27 by 0.32 cm. Weighed and measured samples were loaded into a slotted ZrO_2 refractory brick. Samples were exposed to ten-minute oxidation cycles in stagnant air at 1627 °C. One sample was removed after one cycle, five cycles and ten cycles. A maximum exposure time of 100 minutes was thus achieved. Weight change was measured. X-ray diffraction (XRD) was used to identify oxide phases present after exposure. After surface microstructural analyses by SEM and X-ray energy dispersive spectroscopy (XEDS), samples were cross-sectioned and polished in non-aqueous 1 μm diamond polishing media. Water was avoided to preserve any boria that might be present as an oxidation product. Polished cross-sections were examined using optical and scanning electron microscopy.

Torch Test

Limited oxidation studies were also carried out in a flowing oxyacetylene torch environment. The 2.5 by 2.5 cm by 6 mm thick specimen was mounted in a water cooled picture frame, air-cooled from the back side, and shuttled in and out of an established flame to accumulate thermal cycles. The flame impinged on the HfB_2 coated side. Temperature was monitored with an Ircon R-series two-color optical pyrometer calibrated for the temperature range 980 to 1760 °C. A specimen was exposed to one four minute exposure reaching a maximum temperature of 1805 °C. A second specimen was exposed to three 4-minute cycles attaining temperatures of 1815, 1915, and 2015 °C on the first, second, and third cycles, respectively. Specimens were photographed, and weighed. XRD, optical microscopy, and SEM characterizations were performed.

Results and Discussion

UHTCC Description

The as-received composite plate was non-uniform from front to back surface as shown in figures 1 and 3. The C/SiC surface had a fibrous, uniform appearance; XRD analysis revealed the presence of SiC and C. The HfB_2-rich surface was smooth and non-uniform in appearance with evidence of a coarse grain structure; XRD analysis confirmed the presence of HfB_2. Micro-cracks can be seen in the higher magnification photo of the HfB_2-rich side. With higher magnification SEM, figure 4, the weave pattern on the SiC-rich surface becomes clear. Micro-cracks in the SiC matrix and the HfB_2 coating are now clearly visible. Figure 5 is a light optical microscopy montage across the thickness of the plate. Micro-cracks are present throughout the thickness as one might expect from a carbon fiber reinforced composite with attendant large thermal expansion mismatch between the SiC and HfB_2 matrix phases and the fibers.

The HfB_2 coating layer is comparable in thickness to a fiber ply or about 0.6 mm, and surface micro-cracks were evident.

Figures 6, 7, and 8 are three sets of light optical photomicrographs near the SiC-rich surface, near the center of the plate, and near HfB_2-rich surface, respectively. Each figure contains a series of four photos at increasing magnifications. In figure 6 the lighter gray matrix phase is SiC particulate and the darker gray matrix phase is polymer derived. This is supported by figure 9(a) where the polymer derived phase is identified as Si-O-C. The two photos on the left of figure 7 were taken at the transition from SiC impregnated plies to HfB_2 impregnated plies. Figure 8 focuses on the HfB_2 coating layer and reveals that surface cracks run through the coating thickness. Figure 9(b) shows an area of the coating in more detail. The Si-O-C phase in the matrix is polymer derived. It was not detected by XRD, but it could be amorphous since the pyrolysis temperature was only 850 °C.

Mechanical Properties

Limited four point flexural tests were carried out at span to depth ratios of ~14 and 16 with markedly different results as summarized in tables 1 and 2. Tests were run with the C/SiC or the HfB_2 coated side in tension. At the shorter span to depth failures occurred under a loading pin for both orientations. At a span to depth of 16 failures occurred in the center of the span with fracture initiating in tension, table 1.

Predicted loads for tensile failure were calculated based on beam theory and the rule of mixtures. It was assumed that the matrix made no contribution and that the fibers failed at a tensile strain of 0.7 percent. A fiber tow ultimate strength of 193 GPa was used in the calculations. Predicted loads are compared to observed ultimate loads in table 1. Agreement is remarkably good.

Ultimate flexural strength, strain at ultimate stress, stress and strain at deviation from linear elastic behavior are reported in table 2 and they are summarized in figure 10. Strains at ultimate stress ranged from about 0.6 to 0.7 percent for the C/SiC side in tension, and 0.4 to 0.6 for the HfB_2 side in tension. At constant span to depth the strain at ultimate stress was about 0.2 percent greater for the C/SiC side in tension and the ultimate strength was also higher. Stress versus strain plots are shown in figures 11 and 12. The curves are nonlinear from the start as is typical of a composite with a micro-cracked matrix. The high strains attained before failure and the fact that the specimens remained intact are indicative of composite behavior.

Furnace Oxidation

Photographs of the C/SiC and HfB_2 sides of UHTCC oxidation coupons after exposure to 1, 5 or 10 ten-minute cycles of static furnace oxidation at 1617 °C are shown in figure 13. A non-uniform glassy oxide formed on the C/SiC side. XRD analysis detected SiO_2 as α-cristobalite and SiC. A light colored oxide scale formed on the HfB_2 side. XRD analysis indicated that the scale was $HfSiO_4$ and monoclinic HfO_2. SEM of the oxide scales is shown in figure 14. A porous, microcracked scale formed on the C/SiC side. XEDS results were consistent with identification as SiO_2. A two phase micro-cracked scale formed on the HfB_2 coated side. The angular phase is HfO_2 or $HfSiO_4$ and the amorphous phase is SiO_2.

Weight change data are plotted in figure 15. The interpretation of the data needs to be tempered by the fact that the specimens were cut from a larger plate without providing oxidation protection for the cut edges. This may expose the carbon fibers to rapid attack from the edges. The fibers are also subject to rapid oxidation attack through coating and matrix micro-cracks if these abundant cracks are not rapidly sealed at the exposure temperature by thermal expansion mismatch, and protective oxide scale or glass formation. Finally, AHPCS pyrolysis was only about 95 percent complete. Completion of pyrolysis may account for about 1 percent of additional weight loss.

After one ten-minute exposure the specimens lost about 5 percent of their weight and after one hour of exposure the weight loss was almost 10 percent. The significance of these values will become clearer from metallographic cross-section data.

Metallographic cross-sections of the coupons oxidized at 1627 °C for one, five, and ten cycles are shown in figure 16. On the C/SiC side nearly one, one, and slightly more than one carbon ply were consumed by oxidation after one, five and ten oxidation exposures, respectively. On the HfB_2 coated side of the composite the coating was nearly consumed and carbon attack was less than one ply after 10 cycles. These results indicate that a seal coat is needed on the C/SiC side and a more oxidation resistant coating is required on the UHTC side of the composite.

Along the uncoated edges the depth of fiber consumption was greater by about two times on the C/SiC side as compared to the UHTC side. Disregarding near surface plies, the average depth of fiber attack from the uncoated edge on the C/SiC side was 1.41, 1.47, and 1.64 mm after one, five and ten oxidation exposures, respectively. The average depth of fiber attack from the uncoated edge on the UHTC side was 0.53, 0.73, and 0.68 mm after one, five and ten oxidation exposures, respectively. The sample exposed for one cycle was attacked at only one edge. The other edge was presumably close to the original panel edge and still benefited from the better infiltration that occurs along edges. These results indicate that a seal coat is needed on the cut edges or that cutting should be done prior to completion of fabrication so that a SiC or other protective layer is developed on the cut edges. They also indicate that the HfB_2 phase oxidation products, possibly in combination with SiO_2, are having a beneficial effect with regard to oxidation of the carbon fibers.

A scanning electron micrograph of a specimen cross-section from the specimen exposed for ten ten-minute cycles is shown in figure 17. Elemental dot maps were used to identify phase distributions and these results are shown as labels on the figure. The predominant oxide is $HfSiO_4$ in agreement with XRD results. Isolated particles of SiO_2 and HfO_2 were found. HfB_2 is depleted in the layer shown except for a few large isolated particles.

Torch Tests

A series of photographs of the cool down of the sample exposed to a maximum temperature of 1805 °C for four minutes is shown in figure 18. The temperature versus time history of this specimen during exposure to the oxyacetylene torch flame is given in table 3. Temperature spikes were observed during the test. This is an indication that adherence of the HfO_2-rich scale is an area of concern. The sample exposed for 4 minutes lost 1.9 percent of its initial weight and the sample exposed for three four-minute cycles lost 4.6 wt%.

Only a small area at the center of each coupon was exposed to the highest temperature. The oxidation pattern of the entire coupon and higher magnification views of the center of the coupon exposed for three four-minute cycles are shown in figure 19. The scale formed in the hottest area is light in color and highly micro-cracked. Surface SEM and cross-section metallographic and SEM analyses were performed at the three locations marked by the gold foils on this specimen and at similar locations on the specimen exposed for four minutes. The SEM in figure 20 shows a montage of photographs taken near the center of the specimen exposed for three four-minute cycles. The tip of the foil is at the right of the figure and the center of the specimen is at the left. The oxide scale is micro-cracked and contains pores. SiO_2-rich and HfO_2-rich areas are present. In cooler regions, at Ring A and Ring B as labeled in figure 19, the scales are SiO_2-rich, micro-cracked, and homogeneous in appearance as shown in figure 21**.** Pores are evident in the Ring A scale.

Highlights of the cross-section metallographic and SEM analyses are given in figures 22 and 23. Figure 22 shows cross-sections at the center of the specimens exposed for one and three four-minute cycles. The C/SiC side shows consumption of the carbon fibers to greater than 1 ply after 4 minutes and 2 plies after 12 minutes. The HfB_2 plus Si-O-C coating is nearly totally consumed after 4 minutes and totally consumed after 12 minutes. The extent of coating attack is shown at higher magnification in

figure 23. The outermost dark scale is SiO_2. Below that is a thin band of lighter in appearance HfO_2 and $HfSiO_4$.

Concluding Remarks

Processing

A uniform microstructure was achieved with the C/SiC side having a Si-O-C plus SiC matrix and the UHTC side having a Si-O-C plus HfB_2 matrix. Matrix cracking due to thermal expansion mismatch between the carbon fibers and the matrix constituents is an area of concern.

Mechanical Properties

Flexural strength was close to expected values based on beam theory and the rule of mixtures with no matrix contribution. There was some evidence of composite behavior.

Furnace Oxidation

Based on weight loss, carbon fiber oxidation occurred rapidly with nearly one ply consumed after one ten-minute exposure. After ten ten-minute exposures the carbon consumption slightly exceeded one ply on the C/SiC side and was less than one ply on the UHTC side. This is indicative of some protection afforded by the HfB_2 plus Si-O-C coating layer at 1627 °C. However, this coating layer was nearly consumed after ten furnace exposure cycles. These results indicate that a seal coat is needed on the C/SiC side and a more oxidation resistant coating is required on the UHTC side of the composite. Extensive carbon fiber consumption at cut edges indicates that a seal coat is needed on the cut edges or that cutting should be done prior to completion of fabrication so that a SiC layer is developed on the cut edges. That is, one should strive to produce a net shape part as the final product of processing. HfB_2 slowed the oxidation of the carbon fibers from both the cut edges and from the UHTC coated surface relative to the C/SiC side of the composite.

Torch Test

The UHTCC material withstood ~2000 °C (~3600 °F), severe heat-up and thermal gradients with no major macroscopic distress. Based on observed temperature spikes during test, adherence of the HfO_2-rich scale is an area of concern. Based on metallographic evidence the observed weight losses are attributed primarily to carbon fiber oxidation below the as-produced coupon faces and along cut edges. The HfB2 plus Si-O-C coating layer on the UHTC side of the composite was nearly consumed after one four-minute exposure and was totally consumed after three four-minute exposures.

Recommendations and Future Work

The thermal stress response of this early UHTCC makes the concept worthy of further study. Fiber coatings need to be incorporated to address fiber oxidation issues. Also, advanced SiC fibers need to be evaluated to address oxidation and thermal expansion mismatch issues. Use temperature concerns with SiC fibers are mitigated by the thermo-mechanical loads on a typical leading edge. Compressive stresses

are prevalent at the leading edge and tensile stresses are prevalent in the cooler regions due to a combination of aerodynamic, thermal, and attachment loads. Oxidation resistance can be improved by limiting SiC content, raising the processing temperature to produce purer SiC from the polymeric precursor, and providing HfB_2 or another boron source throughout the composite. Net shape fabrication to avoid machined edges is another important improvement step. We plan to pursue these avenues as continuing development proceeds.

References

1. Bull, J.D., Rasky, D.J., and Karika, C.C., *Stability characterization of diboride composites under high velocity atmospheric flight conditions*. 24th International SAMPE Technical Conference, 1992, pp. T1092–T1106.
2. Clougherty, E.V., Pober, R.L., and Kaufman, L., *Synthesis of oxidation resistant metal diboride composites.* Trans. Met. Soc. AIME, 1968, 242, 1077–1082.
3. Fenter, J.R., *Refractory diborides as engineering materials.* SAMPE Quarterly, 1971, 2, 1–15.
4. Levine, S.R., Opila, E.J., Halbig, M.C., Kiser, J.D., Singh, M., and Salem, J.A., *Evaluation of ultra-high temperature ceramics for aeropropulsion use.* J. European Ceramic Soc., 2002, 22, pp. 2757–2767.
5. Tripp, W.C., Davis, H.H., and Graham, H.C., *Effect of an SiC addition on the oxidation of ZrB_2. Cer*. Bull., 1973, 52, 612–616.
6. Opila, E.J. and Halbig, M.C., *Oxidation of ZrB_2-based ultra-high temperature ceramics*. Ceramic Engineering and Science Proceedings, 2001, 22 # 3, 221–8.
7. Alper, A.M., *High temperature oxides, part II: Oxides of rare earths, titanium, zirconium, hafnium, and tantalum.* Academic Press, New York, 1970. Garvie, R.C., *Zirconium dioxide and some of its binary systems, Chapter IV*. Lynch, C.T., *Hafnium oxide*, Chapter VI.
8. Anon., *Engineering property data on selected ceramics, Vol. III, Single oxides*. MCIC-HB-07, Battelle, Columbus, OH, 1981.
9. Hurwitz, F.I., *Filler/polycarbosilane systems as cmc matrix precursors*, *Ceram. Eng. Sci. Proc.,* 19(3) 267–274 (1998).
10. ASTM C 1161–00, *Standard test method for flexural properties of continuous fiber-reinforced advanced ceramic composites*. Annual Book of ASTM Standards, V. 15.01, American Society for Testing and Materials, West Conshohocken, Pennsylvania (2002).

Table 1. Flexural tests and ultimate load results.

Specimen			Test Fixture			Orientation		Ultimate Load, N	Calculated Load Based on Beam Theory,* N
ID	width, mm	thickness, mm	inner span, mm	outer span, mm	span/ depth	fracture	side down		
A	12.71	5.79	40	80	13.8	under pin	C/SiC	972	1120
B	12.65	5.92	40	80	13.5	under pin	UHTC	757	
C	12.66	6.04	48	96	15.9	center	C/SiC	1025	1000
D	12.66	6.06	48	96	15.8	center	UHTC	811	
E	12.66	6.07	48	96	15.8	center	UHTC	855	

Table 2. Flexural test stress and strain results.

Test			Results					
ID	~ Span / Depth	Tensile Side	ultimate flexural strength, MPa	ultimate strain (crossh'd), %	deviation from linearity, MPa	strain at dfl, %	deviation from linearity, MPa	strain at dfl, %
					crosshead strain basis		deflectometer strain	
A	14	C/SiC	137.0	0.59	26.4	0.105		
B	14	UHTC	102.3	0.39	31.4	0.113		
C	16	C/SiC	161.8	0.73	28.2	0.078	23.0	0.058
D	16	UHTC	136.7	0.56	24.7	0.056	26.0	0.059
E	16	UHTC	131.8	0.55	26.1	0.090	26.1	0.063

Table 3. Oxy-acetylene torch test cycle one temperature history

Time, min.	Temp, °C
0.5	1720
1.0	1750
1.5	1750
2.0	1755
2.5	1765
3.0	1775
3.5	1790
4.0	1805

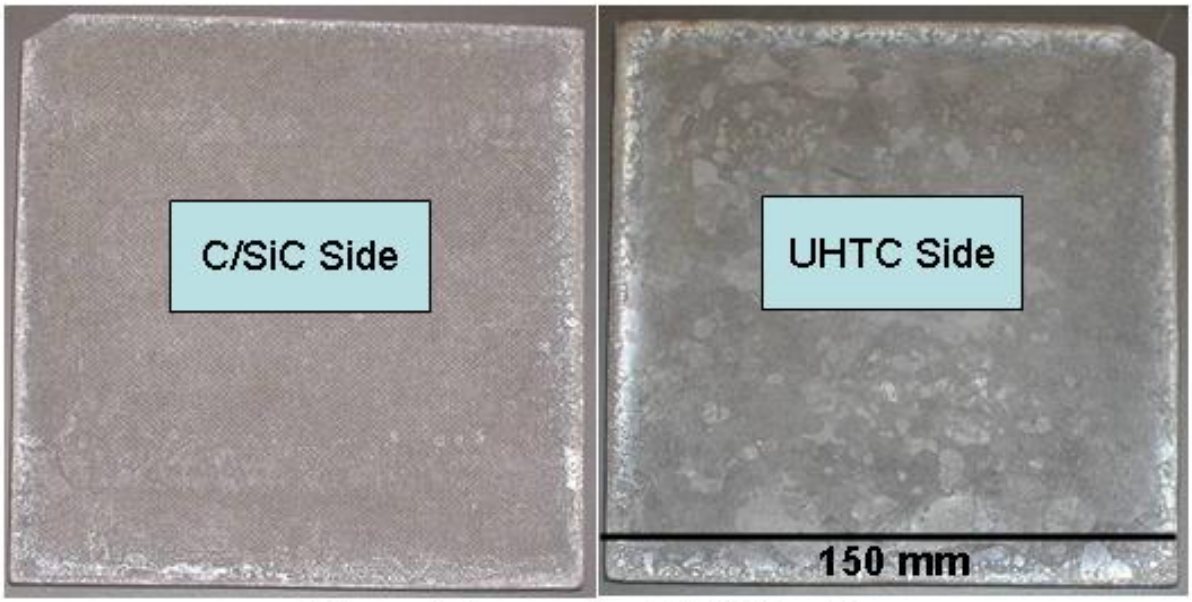

Figure 1. As-received UHTCC plate

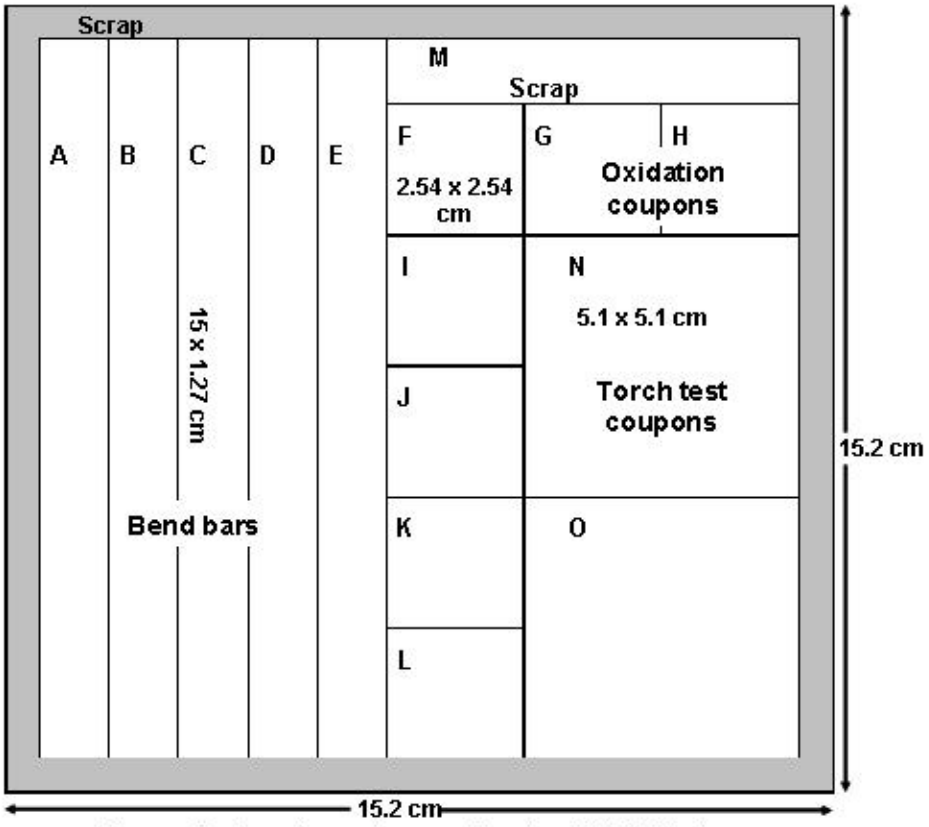

Figure 2. Specimen lay-out for the UHTCC plate.

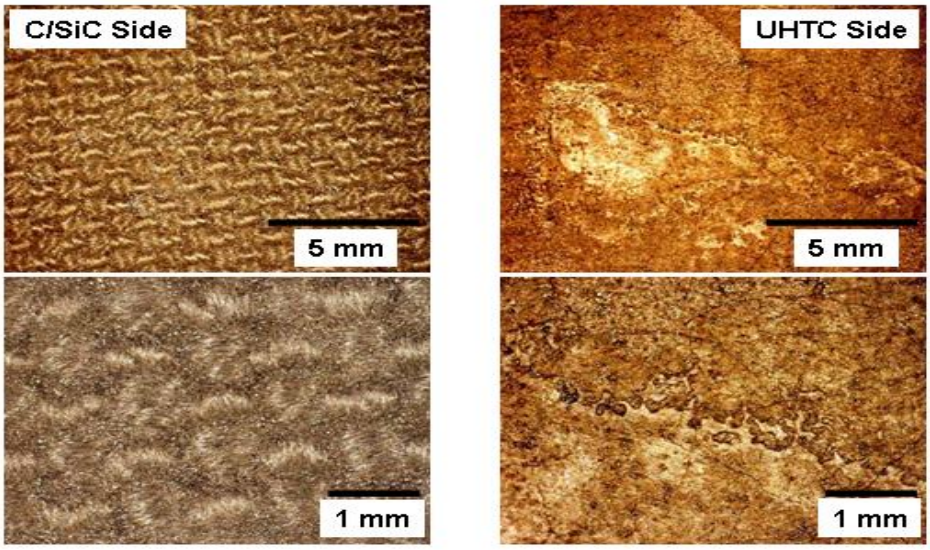

Figure 3. Macrophotographs of UHTCC plate.

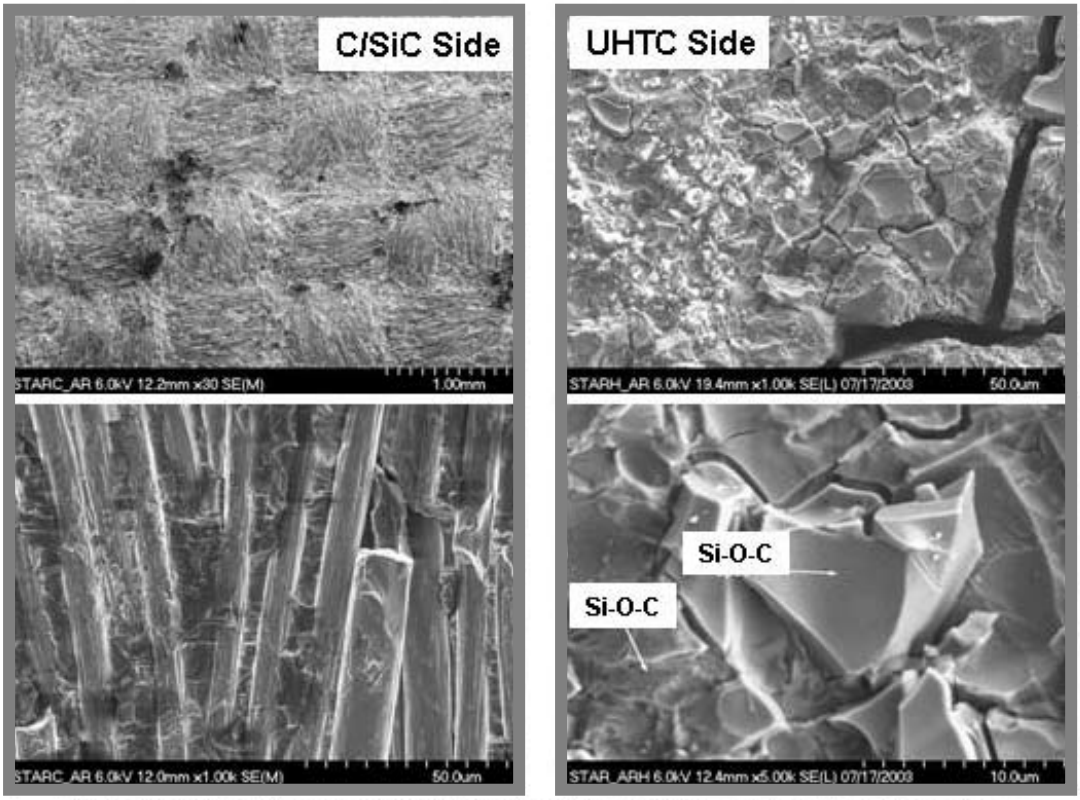

Figure 4. FESEM micrographs of the as-received UHTCC plate.

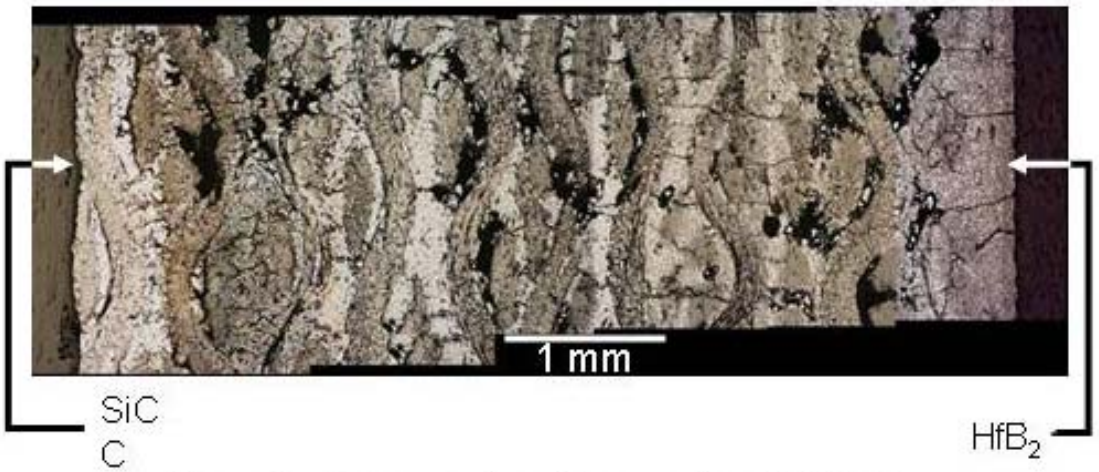

Figure 5. Cross-section of as-received UHTCC plate and surface phases detected by XRD.

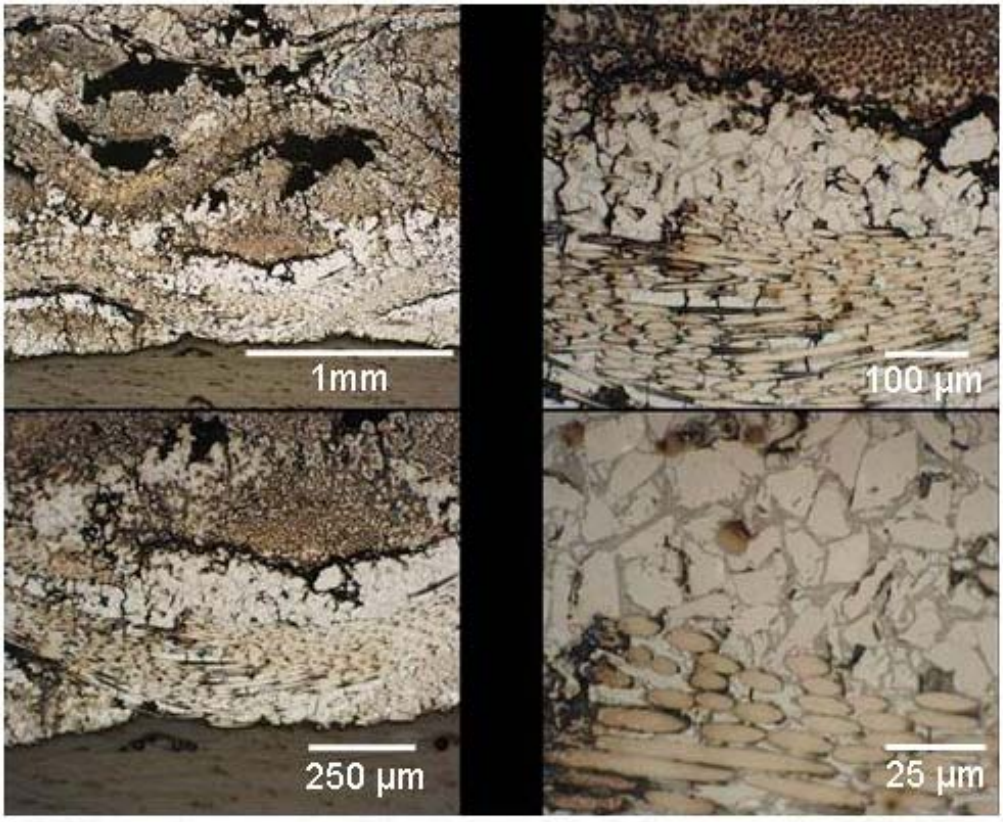

Figure 6. Photomicrographs of the C/SiC side of the as-received UHTCC plate.

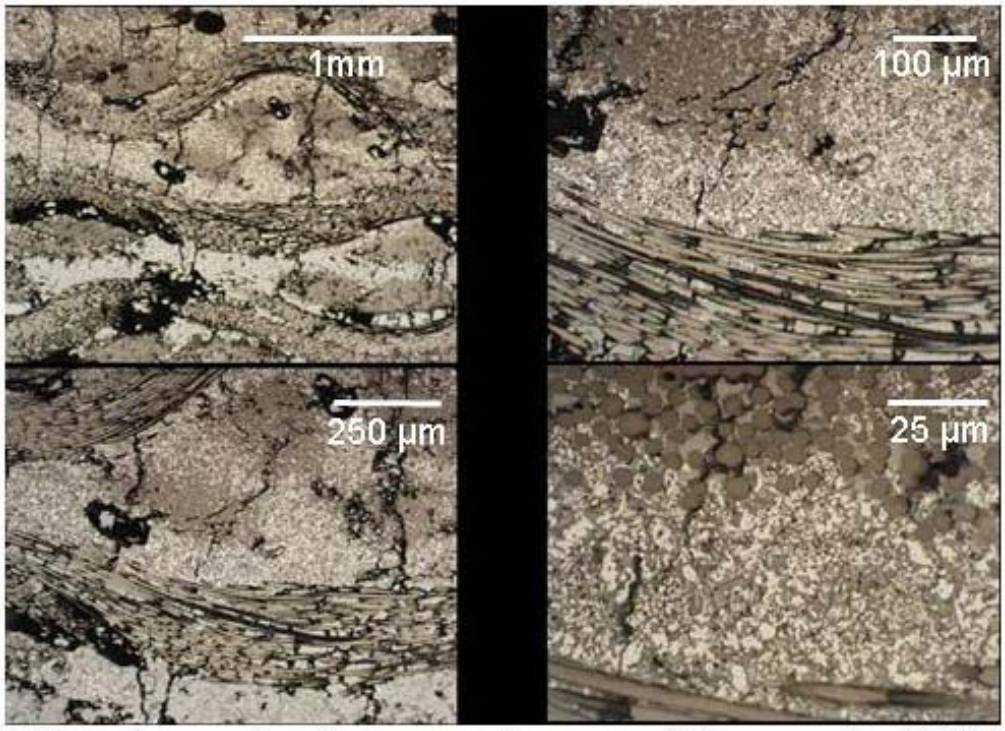

Figure 7. Photomicrographs of areas near the center of the as-received UHTCC plate.

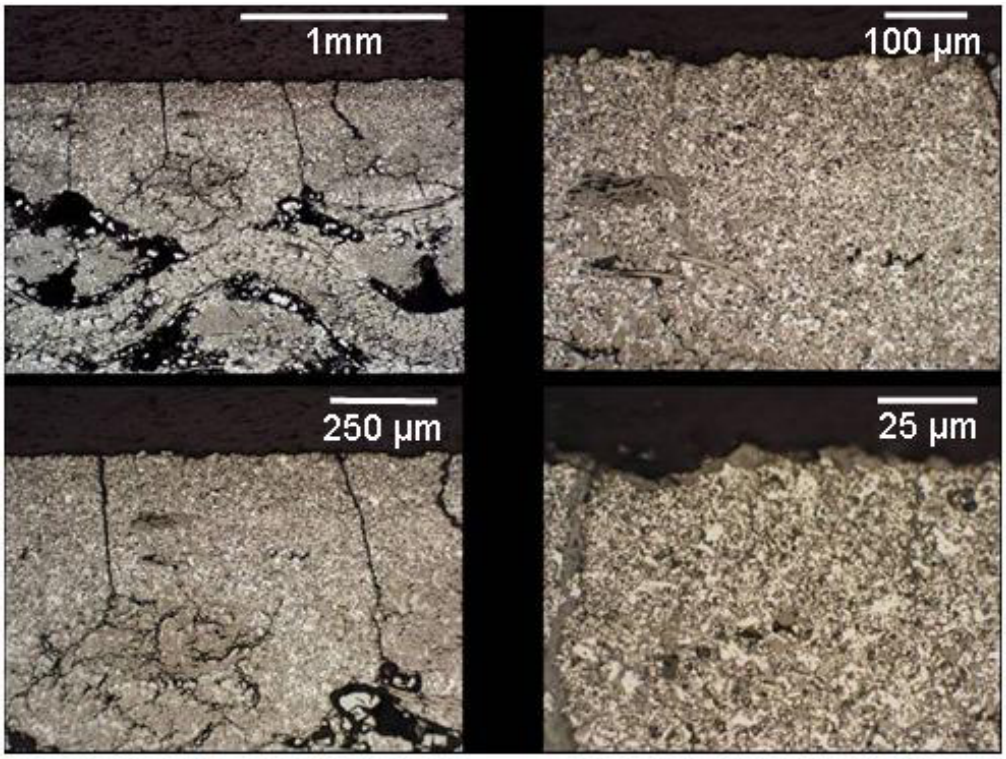

Figure 8. Photomicrographs of the HfB_2 side of the as-received UHTCC plate.

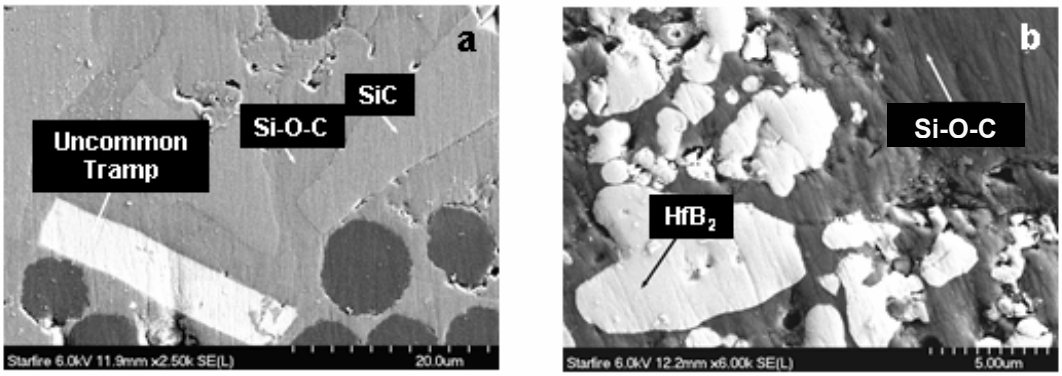

Figure 9. FESEM photomicrographs and EDS identifications of phases present in the as-received UHTCC plate. (a) Matrix on the C/SiC side. (b) HfB_2 coating layer.

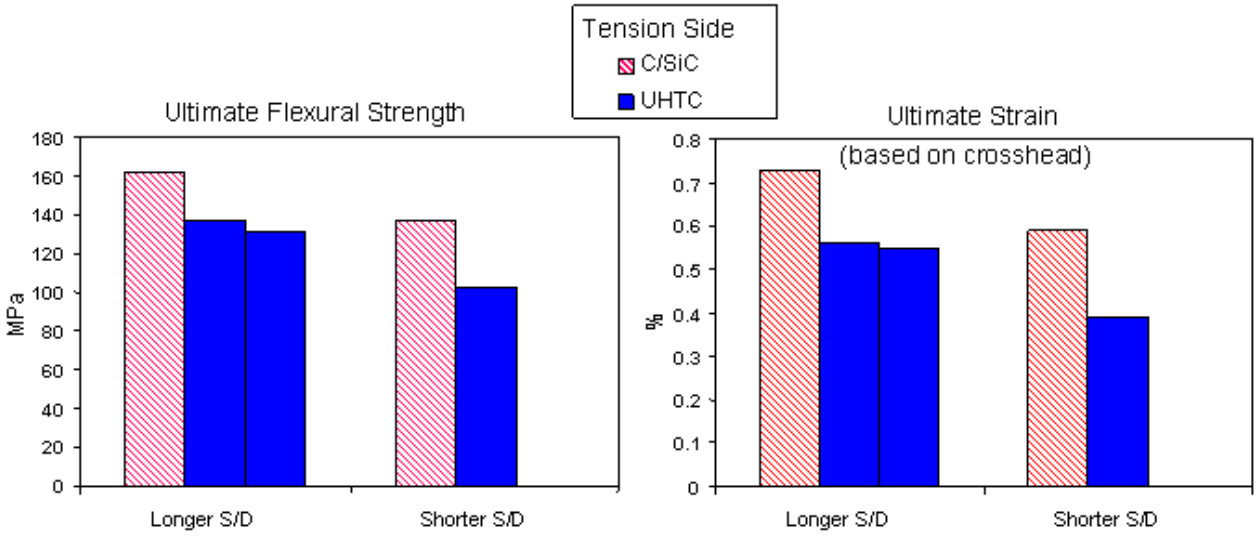

Figure 10. UHTCC flexural strength test results

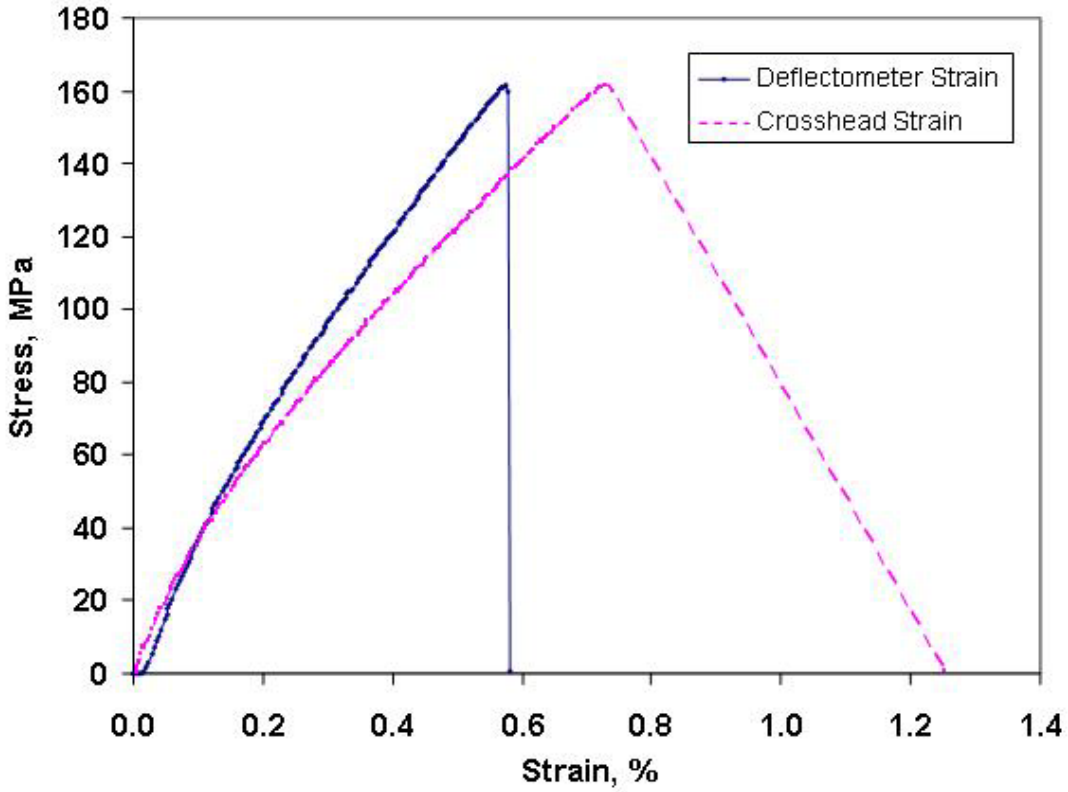

Figure 11. Sample C tested with the C/SiC side in tension and a span / depth ration of ~ 16.

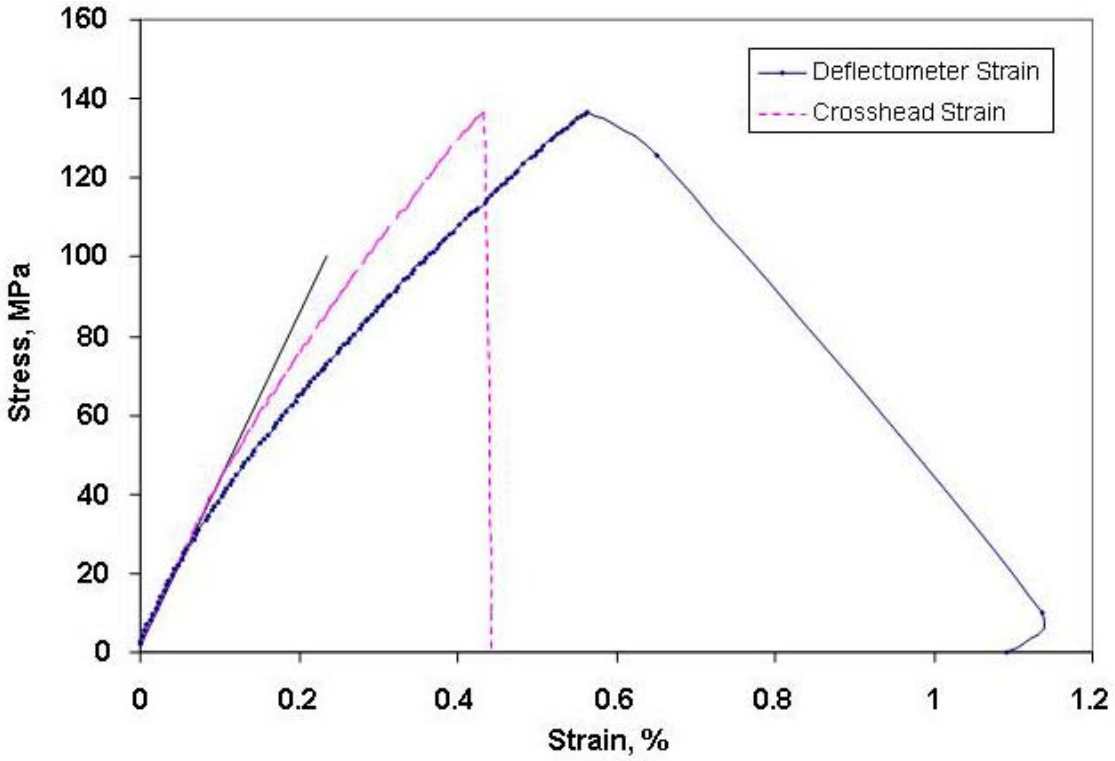

Figure 12. Sample D tested with the UHTC side in tension and a span / depth ration of ~ 16.

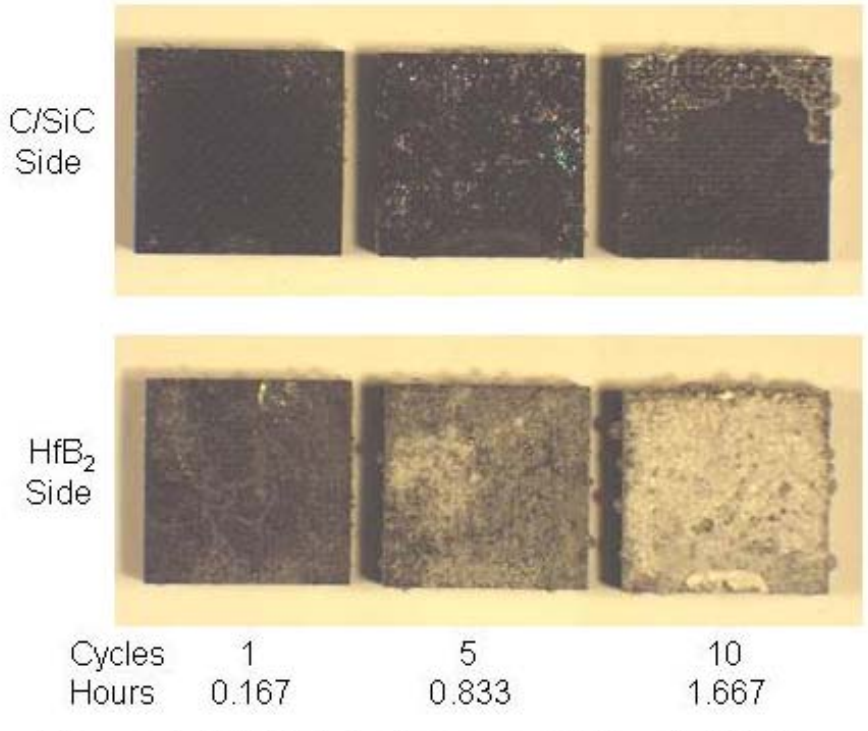

Figure 13. UHTCC after furnace oxidation at 1627 °C.

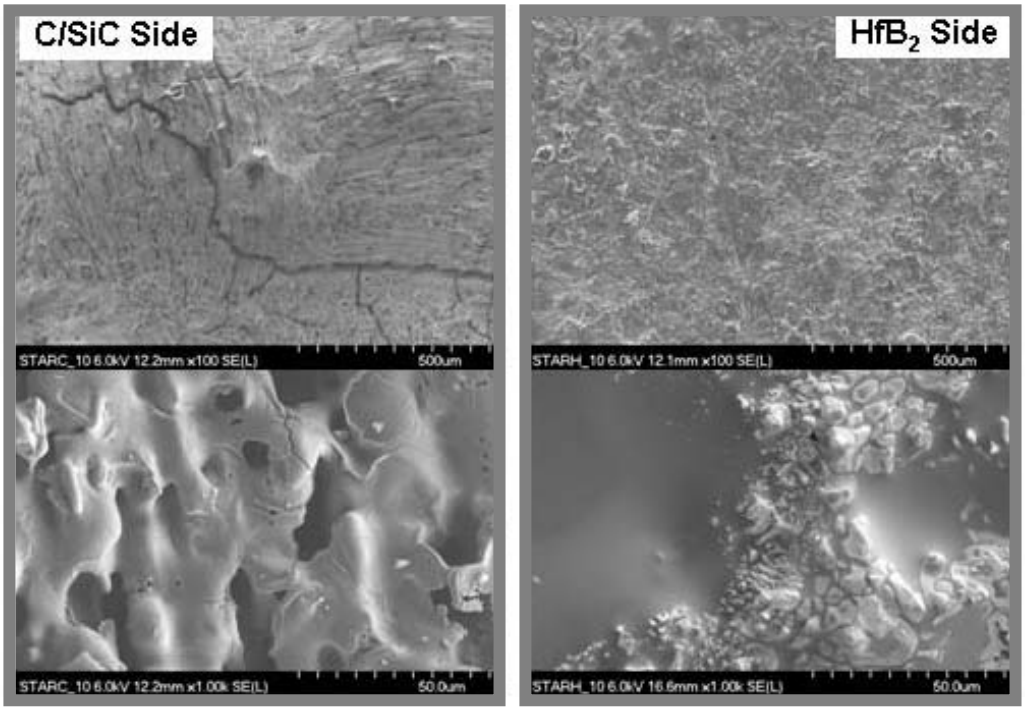

Figure 14. FESEM micrographs of UHTCC after exposure in air furnace oxidation at 1627 °C.

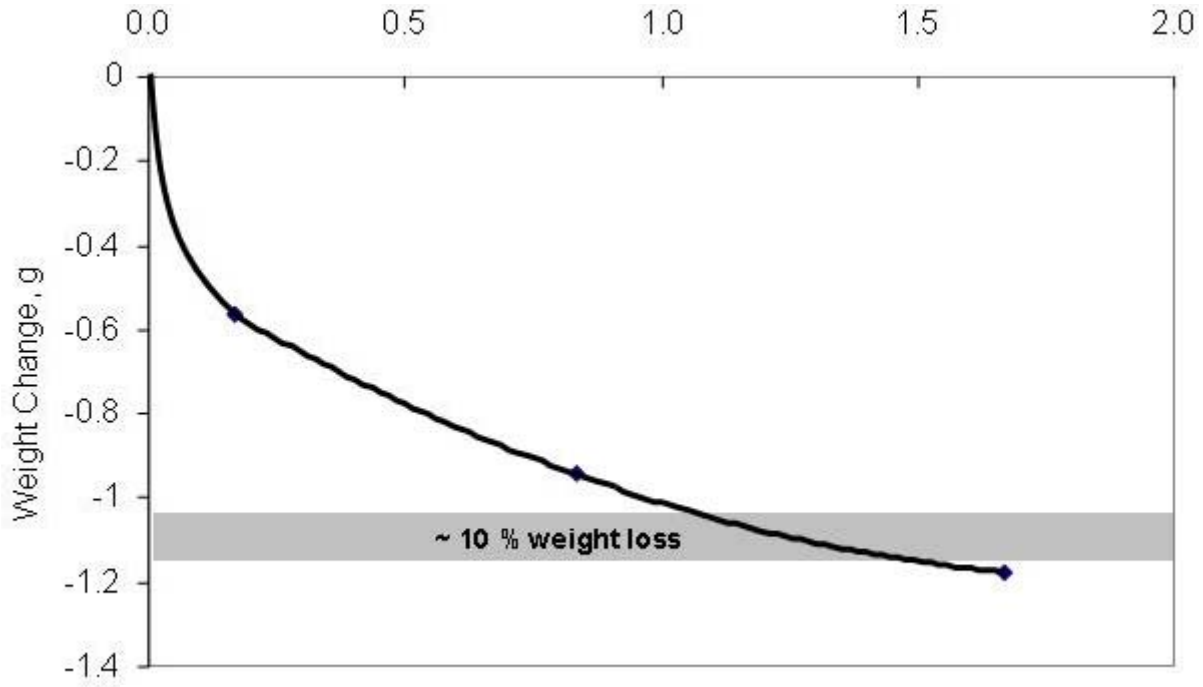

Figure 15. 1627 °C furnace oxidation weight change for UHTCC.

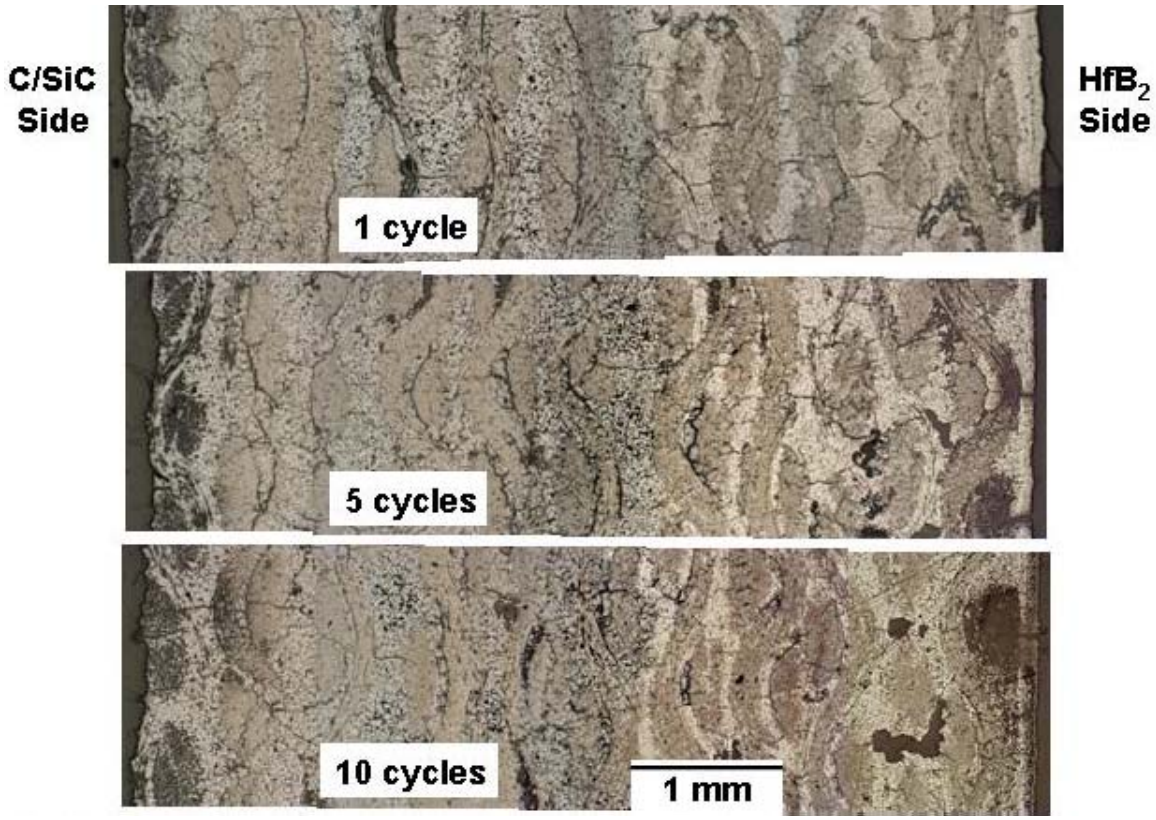

Figure 16. UHTCC composite after ten-minute furnace exposure cycles to 1627 °C. Thickness differences are due to oxidation and variations in plate thickness.

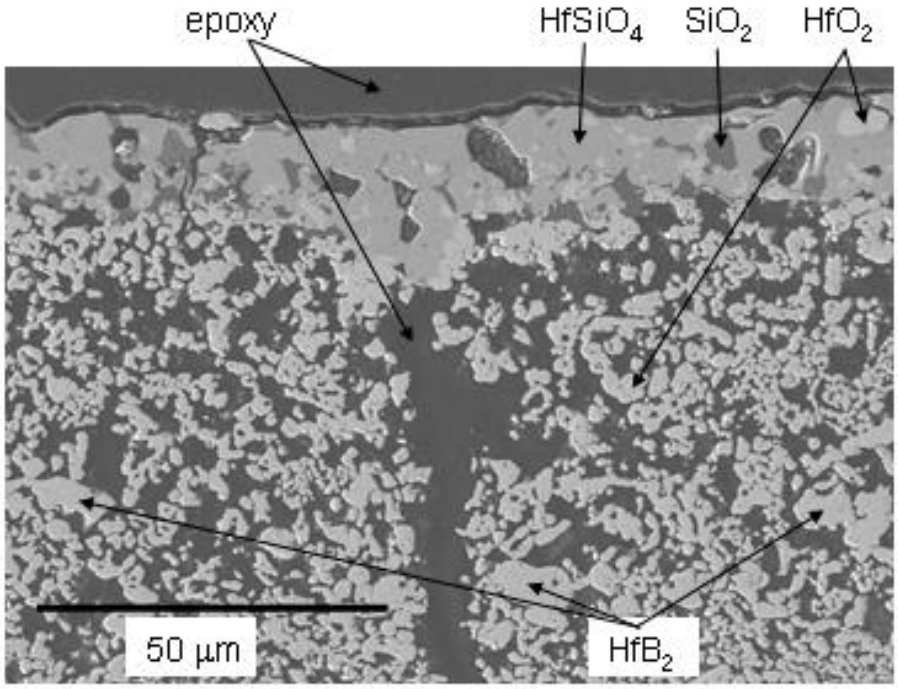

Figure 17. UHTCC composite after 10 ten-minute furnace exposure cycles to 1627 °C in air. The oxidized surface, originally HfB_2-rich, is shown. The surface oxide is primarily $HfSiO_4$, with some areas of HfO_2 and SiO_2. Beneath this layer, all brightly contrasting particles are HfO_2 except the three larger particles specifically labeled as HfB_2.

Figure 18. Photographs of specimen “O” during cool-down from 1805 °C oxy-acetylene torch test.

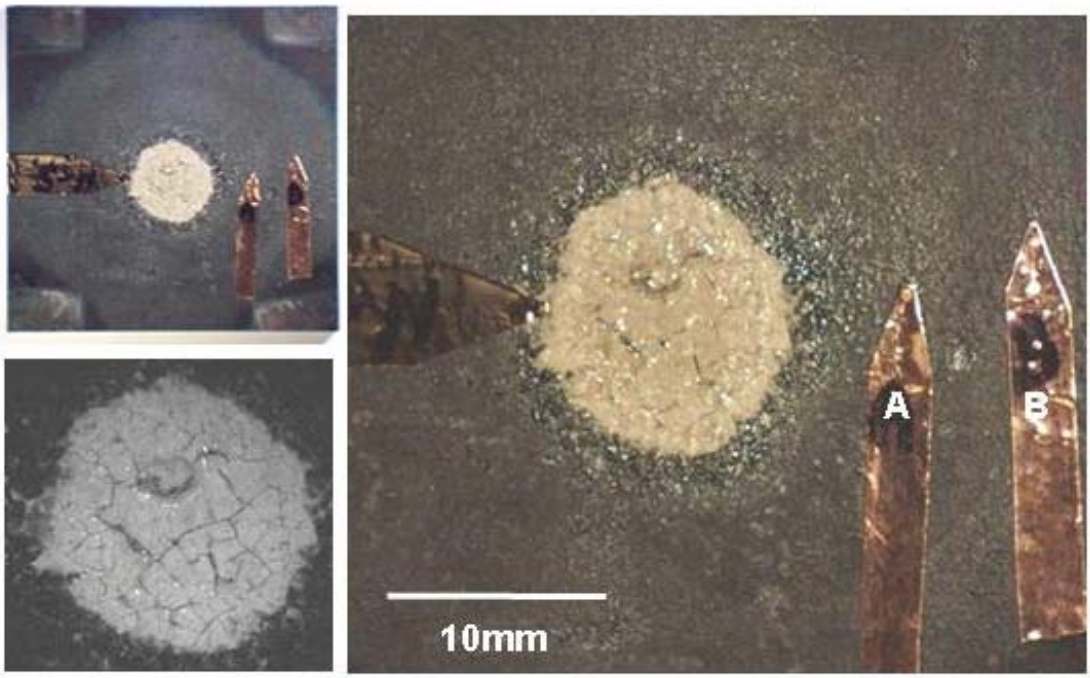

Figure 19. Photographs of UHTCC specimen “N” after three four-minute torch cycles to 1815 to 2015 ^{o}C. Gold foils indicate locations where FESEM microscopy and EDS were performed.

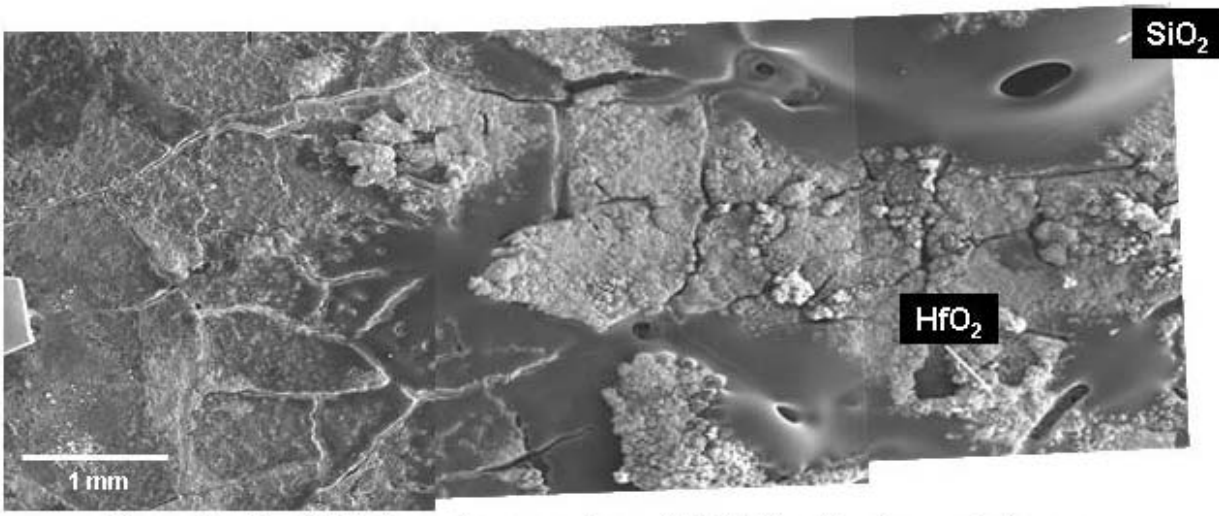

Figure 20. FESEM photomicrographs and EDS identifications of phases present on the center of the UHTCC surface after three torch cycles.

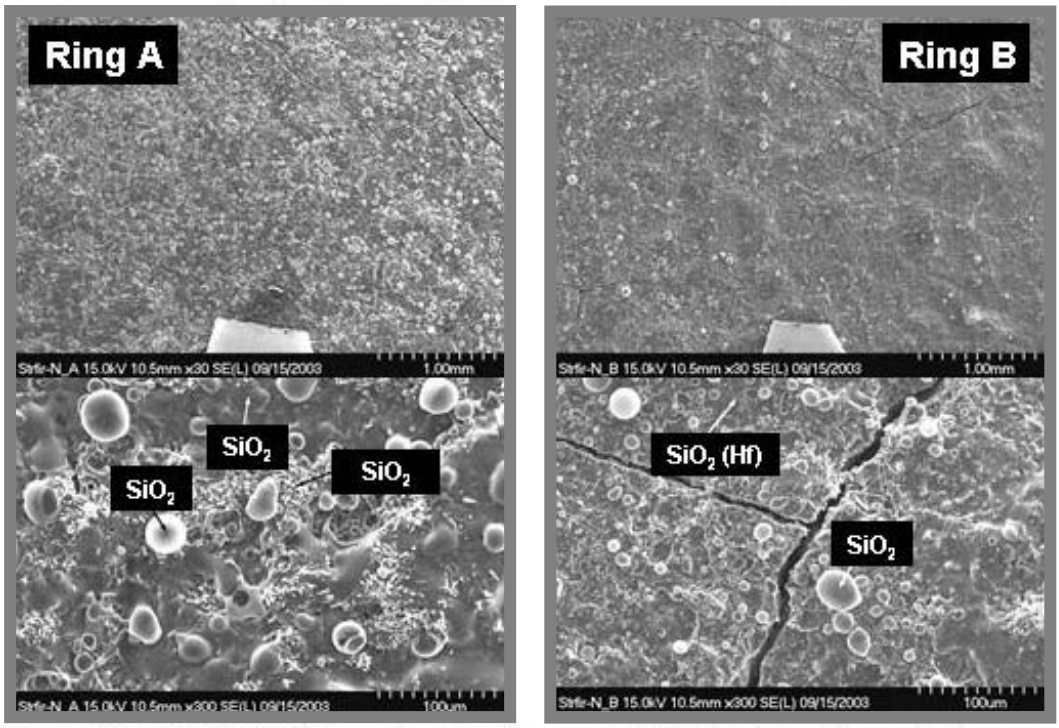

Figure 21. FESEM photomicrographs and EDS identifications of phases present at Ring A and Ring B of the UHTCC surface after three torch cycles.

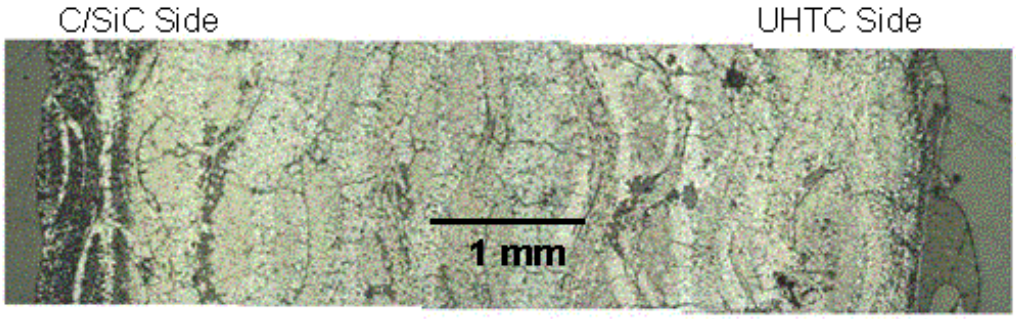

a. One 4-minute cycle to 1805 °C.

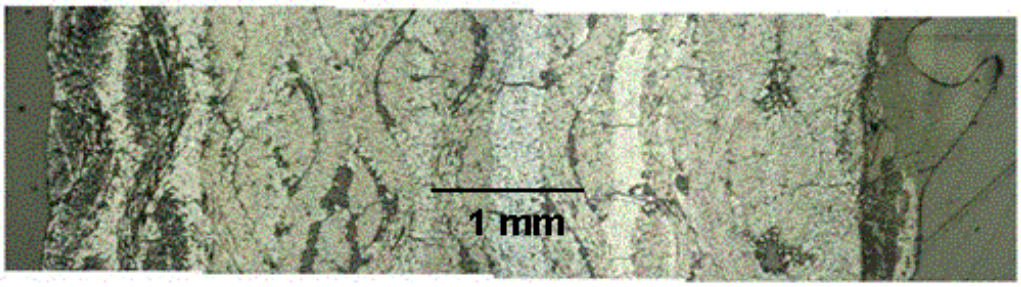

b. Three 4-minute cycles to 1815 to 2015 °C.

Figure 22. UHTCC torch test specimen center cross-sections.

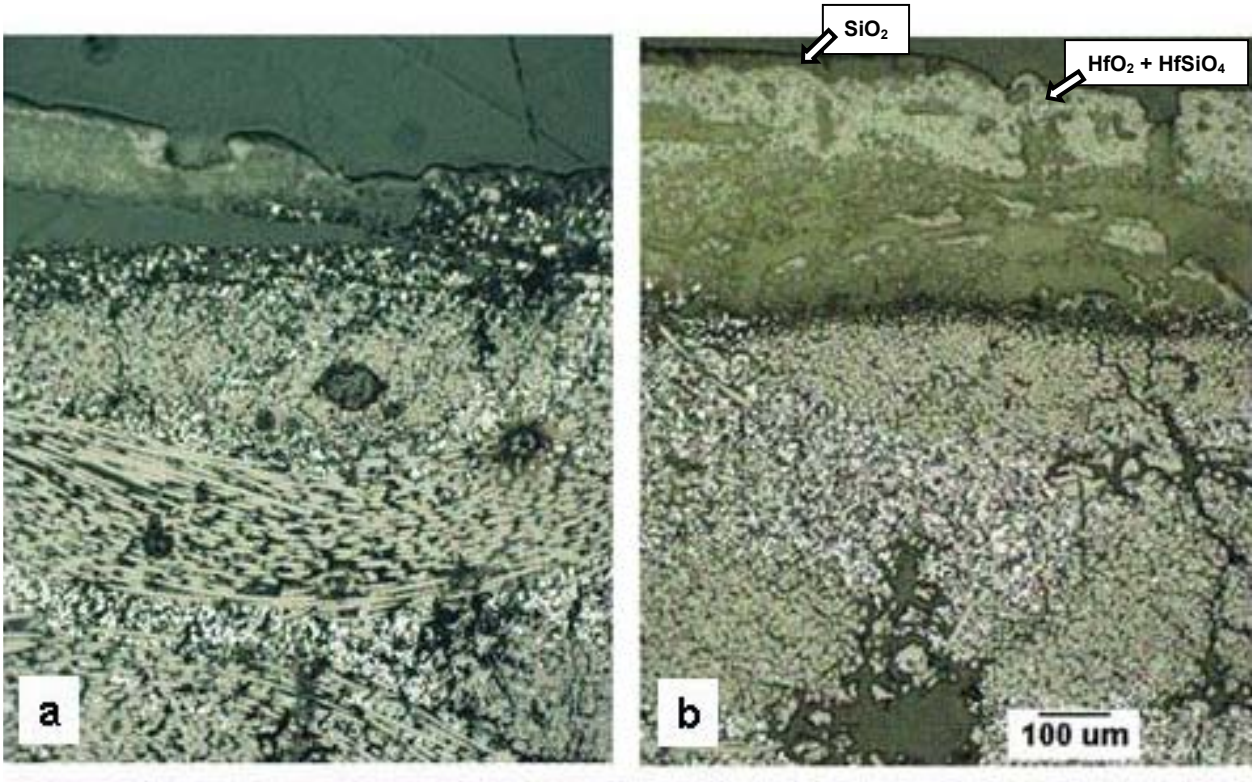

Figure 23. UHTCC torch test specimen cross-sections at center of hot side. (a) After one 4-minute cycle to 1805 ^{o}C. (b) After three 4-minute cycles to 1815 to 2015 ^{o}C.

REPORT DOCUMENTATION PAGE

Form Approved
OMB No. 0704-0188

1. AGENCY USE ONLY (*Leave blank*)	2. REPORT DATE	3. REPORT TYPE AND DATES COVERED
	May 2004	Technical Memorandum

4. TITLE AND SUBTITLE

Characterization of an Ultra-High Temperature Ceramic Composite

5. FUNDING NUMBERS

WBS–22–794–40–4S

6. AUTHOR(S)

Stanley R. Levine, Elizabeth J. Opila, Raymond C. Robinson,
and Jonathan A. Lorincz

7. PERFORMING ORGANIZATION NAME(S) AND ADDRESS(ES)

National Aeronautics and Space Administration
John H. Glenn Research Center at Lewis Field
Cleveland, Ohio 44135–3191

8. PERFORMING ORGANIZATION REPORT NUMBER

E–14563

9. SPONSORING/MONITORING AGENCY NAME(S) AND ADDRESS(ES)

National Aeronautics and Space Administration
Washington, DC 20546–0001

10. SPONSORING/MONITORING AGENCY REPORT NUMBER

NASA TM—2004-213085

11. SUPPLEMENTARY NOTES

Stanley R. Levine and Elizabeth J. Opila, NASA Glenn Research Center; Raymond C. Robinson, QSS Group, Inc., 21000 Brookpark Road, Cleveland, Ohio 44135; and Jonathan A. Lorincz, Ohio University, Main Campus, 1 Ohio University, Athens, Ohio 45701. Responsible person, Stanley R. Levine, organization code 5130, 216–433–3276.

12a. DISTRIBUTION/AVAILABILITY STATEMENT

Unclassified - Unlimited
Subject Category: 23 Distribution: Nonstandard

Available electronically at http://gltrs.grc.nasa.gov

This publication is available from the NASA Center for AeroSpace Information, 301–621–0390.

12b. DISTRIBUTION CODE

13. ABSTRACT ***(Maximum 200 words)***

Ultra-high temperature ceramics (UHTC) are of interest for hypersonic vehicle leading edge applications. Monolithic UHTCs are of concern because of their low fracture toughness and brittle behavior. UHTC composites (UHTCC) are being investigated as a possible approach to overcome these deficiencies. In this study a small sample of a UHTCC was evaluated by limited mechanical property tests, furnace oxidation exposures, and oxidation exposures in a flowing environment generated by an oxy-acetylene torch. The composite was prepared from a carbon fiber perform using ceramic particulates and a preceramic polymer. Test results raised concerns about microcracking due to thermal expansion mismatch between the matrix and the carbon fiber reinforcements, and about the oxidation resistance of the HfB_2-SiC coating layer and the composite constituents. However, positive performance in the torch test warrants further study of this concept.

14. SUBJECT TERMS

Ceramic composites; Oxidation; Refractory materials

15. NUMBER OF PAGES

26

16. PRICE CODE

17. SECURITY CLASSIFICATION OF REPORT	18. SECURITY CLASSIFICATION OF THIS PAGE	19. SECURITY CLASSIFICATION OF ABSTRACT	20. LIMITATION OF ABSTRACT
Unclassified	Unclassified	Unclassified	